



The ECMWF land surface scheme extended with a photosynthesis and LAI module tested for a coniferous forest site

*M.H. Voogt, B.J.J.M. van den Hurk and
C.M.J. Jacobs*

Koninklijk Nederlands Meteorologisch Instituut



De Bilt, 2006

PO Box 201
3730 AE De Bilt
Wilhelminalaan 10
De Bilt
The Netherlands
<http://www.knmi.nl>
Telephone +31(0)30-220 69 11
Telefax +31(0)30-221 04 07

Authors: Voogt, M.H.
Hurk, B.J.J.M. van den
Jacobs, C.M.J. (WUR – Alterra)

The ECMWF land surface scheme extended with a photosynthesis and LAI module tested for a coniferous forest site

M.H. Voogt ^a, B.J.J.M. Van den Hurk ^a and C.M.J. Jacobs ^b

^a Royal Netherlands Meteorological Institute, PO Box 201, 3730 AE De Bilt, The Netherlands

^b Alterra, PO Box 47, 6700 AA Wageningen, The Netherlands

kanmunt 2008

36

8

11

Abstract

The stomatal conductance scheme and vegetation evolution module that are employed in the ISBA-A-gs soil-vegetation-atmosphere transfer model, are implemented in the ECMWF land surface scheme TESSEL. The new scheme, called C-TESSEL, is able to simulate carbon fluxes and to calculate LAI dynamically. C-TESSEL is tested for a coniferous forest site in the Netherlands. Simulated carbon and latent heat fluxes are validated against micrometeorological observations. The latent heat flux is simulated with acceptable accuracy, both with respect to observations and to simulations by the unmodified TESSEL model. However, it is shown that the quality of the simulated carbon fluxes is not sufficient to allow the present configuration of C-TESSEL to be used in a data assimilation system. A general sensitivity analysis on three vegetation type specific parameters indicates that the simulated latent heat flux is highly sensitive to the presence of vegetation via the leaf nitrogen content and - when vegetation is not limited - also to the soil moisture conditions. The latent heat flux turns out to be insensitive to the parameter chosen to represent the influence of the photosynthetic activity (mesophyll conductance under unstressed soil moisture conditions) due to compensating effects of associated parameters concerning the effect of humidity deficit on stomatal conductance. The sensitivity analysis also shows that for the coniferous forest site, C-TESSEL is not able to simulate both the right magnitude of the latent heat flux and the day-to-day variability with a given set of parameter values.

1 Introduction

The greenhouse gas CO_2 plays an important role in the radiation budget of the earth. Its concentration has increased significantly since the 18th century because of anthropogenic emissions. The CO_2 concentration is influenced by the exchange of carbon between the terrestrial biosphere and the atmosphere. Present and future surface carbon fluxes are boundary conditions for the evolution of the atmospheric CO_2 concentration. Estimates of carbon fluxes and their evolution at a global scale are uncertain (Houghton et al., 2001). In particular, with regard to projections of the future climate, several studies indicate that the current carbon sink in the terrestrial biosphere may turn into a source, but uncertainties are large (Cox et al., 2000; Cramer et al., 2001; Friedlingstein et al., 2003).

Studies have been carried out in order to improve the understanding of the processes involved in the terrestrial exchange of carbon. Recently, in the framework of the Project for Intercomparison of Land surface Parameterization Schemes for Carbon (PILPS-C1), a land surface model intercomparison experiment was performed for both energy and carbon fluxes (Viovy, 2002). Other studies are designed to build data assimilation systems in which modelled and observed information are combined within a consistent framework. Within the context of the Carbon Assimilation and Modelling of the European Land Surface (CAMELS) project, part of the CarboEurope cluster of projects (Hofmann, 2006), a Carbon Cycle Data Assimilation System (CCDAS) was developed, assimilating atmospheric CO_2 concentration observations and satellite observations of photosynthetically active radiation (PAR) into a global climate model (Rayner et al., 2005; Knorr and Cox, 2004).

In this paper, we present the first results of modelling carbon fluxes and leaf area index (LAI) dynamics with the operational land surface model of the European Centre for Medium-range Weather Forecasts (ECMWF). The present study is carried out prior to the development of a global monitoring system for carbon fluxes and atmospheric CO_2 concentrations. In this monitoring system, observations related to the terrestrial carbon cycle (primarily vegetation data) are integrated in a land surface model through data assimilation. An assessment of the skill of the land surface model is needed before it can serve in a system for assimilating terrestrial carbon related data. This paper focuses on this assessment.

The standard version of the Tiled ECMWF Scheme for Surface Exchanges over Land (TESSEL) was introduced in the year 2000 and used in the ERA40 re-analysis (Van den Hurk et al., 2000). It does not account for the exchange of carbon, nor does it represent vegetation in a dynamic way. Plant transpiration is controlled by an empirical parameterization of the stomatal conductance, which assumes that environmental factors have an independent control on the conductance. The stomatal conductance is scaled up to the canopy level by multiplying with the leaf area index (LAI). Vegetation type specific values of LAI are prescribed using land surface databases but do not have a seasonal variation.

The uptake and release of carbon by the vegetation and soil interacts with the exchange of energy, moisture and momentum between the land surface and the atmosphere. Plants open their stomata to assimilate CO_2 and evaporate water simultaneously. The stomatal conductance involved in these processes depends on the meteorological conditions as well as vegetation and soil conditions. In what is often called an A-gs scheme, the canopy conductance is derived from a photosynthesis model. Interactions between radiation, temperature and CO_2 concentration are then taken into account. The dependence on the atmospheric CO_2 concentration makes such models suitable for use in climate change studies. The A-gs scheme proposed by Jacobs (1994) has been implemented in the ISBA (Interactions between Soil, Biosphere and Atmosphere) land surface model, coupled with a vegetation evolution scheme (Calvet et al., 1998). Vegetation type specific parameter values for ISBA-A-gs were obtained by a meta-analysis (Calvet, 2000; Calvet et al., 2004) and were slightly adapted to optimize global LAI simulations (Gibelin et al., 2006). For the present study, the A-gs and vegetation

evolution modules from ISBA-A-gs are implemented in TESSEL. C-TESSEL refers to this new version of the ECMWF land surface model.

In this paper we assess whether C-TESSEL has enough skill to be able to be used in a system to monitor CO₂ fluxes and latent heat fluxes for a coniferous forest site in the Netherlands. For that purpose, C-TESSEL is run in a stand alone mode (outside a data assimilation system). We require that the model simulates realistic diurnal and seasonal variation in the net ecosystem CO₂ exchange (NEE). The model needs to respond to conditions in the atmosphere, vegetation and soil in a realistic way. When running C-TESSEL in a data assimilation system, the required systematic increments induce a permanent non-physical term in the energy and mass balance. Therefore, large deviations from the observations are not desirable. We compare normalized RMSE values with the observational uncertainty or variability in order to test this.

We start with a description of C-TESSEL and the components on which it is based in Section 2. The data sets and statistical methods with which we validate the hypothesis above are presented in Section 3. In Section 4 results from a validation exercise in which vegetation parameter values are used that are globally tuned for ISBA-A-gs are presented. The C-TESSEL simulation of the NEE in the period 1997-1999 is compared to flux tower measurements. The simulation of the daytime latent heat flux is also compared to the TESSEL simulation. In Section 5, a general sensitivity analysis is performed for three vegetation parameters that are assumed to be crucial for the simulation of the latent heat flux (mesophyll conductance, critical soil moisture index and leaf nitrogen content). This analysis indicates whether the current coniferous forest parameter set of C-TESSEL is robust. Finally, in Section 6 the conclusions and directions for future research are presented.

2 Model description

2.1 TESSEL

TESSEL is a tiled land surface scheme which has been used in the ECMWF Numerical Weather Prediction (NWP) model since the year 2000 (Van den Hurk et al., 2000). TESSEL allows one low and one high vegetation tile per grid box, thus only dominant vegetation types within the grid box are accounted for. The other sub-grid fractions over land represent bare soil, interception, snow on low vegetation/bare soil and snow underneath high vegetation. As indicated before, the stomatal conductance is calculated using the Jarvis-type parameterization (Jarvis, 1976). It is scaled up to the canopy level by multiplication with the LAI. Values of the LAI are prescribed using land surface databases but do not have a seasonal variation. Regarding the soil parameterization, TESSEL has four soil layers extending to a depth of 2.89 m. It has a medium soil texture that is uniform across the globe.

2.2 ISBA-A-gs

ISBA-A-gs is the CO₂-responsive version of the land surface model ISBA (Calvet et al., 1998). The model simulates the stomatal conductance based on the A-gs scheme proposed by Jacobs (1994), in which stomatal aperture depends on photosynthetic rate. The model includes a biomass evolution module. The growth of active biomass (leaves) directly depends on net CO₂ assimilation, whereas the mortality decline is based on an exponential time evolution whose e-folding time depends on the daily maximum net CO₂ assimilation. During the growing period, a nitrogen dilution equation is used to relate above-ground structural biomass to active biomass and vice versa (Calvet and Soussana, 2001). The LAI is related to

the active biomass B via the following relationship:

$$\frac{B}{LAI} = \frac{1}{eN_a + f} \quad (1)$$

where the leaf nitrogen concentration N_a and two plasticity parameters e and f are vegetation type specific parameters. Nitrogen is a building block for plant growth and LAI is enhanced by high values of N_a . The LAI has a prescribed minimum value. Through the dynamic representation of the LAI, the model can account for seasonal and interannual variability, responding to e.g. droughts (Bonan, 1998). Wood and soil carbon reservoirs are not included in the biomass evolution module.

Soil moisture stress affects the stomatal aperture. The A-gs scheme by Jacobs (1994) was extended in ISBA-A-gs to include responses to soil moisture. Plants tend to respond to soil moisture stress in two different ways (Calvet, 2000; Calvet et al., 2004). Some plant types try to avoid stress, by reducing the transpiration via stomatal regulation. This stress strategy is typified as defensive. In contrast, others apply an offensive strategy suppressing stress by a more efficient root water-uptake or a more rapid growing cycle. In both strategies, two stress regimes are distinguished, separated by a critical soil moisture index value. The stress strategies are applied differently by high and low vegetation types. In Section 2.4, the stress regulation is described in more detail.

The model is forced by the ECOCLIMAP global surface parameter database (Masson et al., 2003). ECOCLIMAP distinguishes 9 vegetation types that are grouped into 7 vegetation classes with respect to photosynthetic behaviour. There are 3 classes for high vegetation (deciduous, coniferous and evergreen forests) and 4 classes for low vegetation (C3 grass, C3 crops, C4 grass, C4 crops), each having a distinctive set of vegetation parameter values. Calvet (2000) and Calvet et al. (2004) calibrated the parameter values using data from a large number of species by optimizing the simulated water fluxes. The mean values were slightly adapted to optimize global LAI simulations (Gibelin et al., 2006).

2.3 C-TESSEL

C-TESSEL refers to the implementation of the A-gs and vegetation evolution modules from ISBA-A-gs in TESSEL. The original number of vegetation tiles in TESSEL was increased to represent the 7 vegetation classes from ISBA-A-gs. In that way, not only dominant vegetation types are accounted for. Only one tile with snow underneath high vegetation is kept, and the dominant high vegetation type is assigned to it. It is assumed that wet leaves assimilate CO_2 in the same way as dry leaves, since the stomata are generally located at the lower side of the leaves. Snow-covered vegetation does not assimilate CO_2 . The minimum e-folding time in the biomass decline calculation is constrained to 10% of the maximum value in order to avoid unrealistically high loss of vegetation biomass when CO_2 assimilation is low. At present, a constant value of 353 ppm is assumed to represent the ambient CO_2 concentration.

NEE is the sum of the gross CO_2 assimilation (A_g) and the CO_2 ecosystem respiration (R_{eco}). R_{eco} is split into two terms. The first is dark respiration (R_d), the autotrophic respiration from the leaves. In order to sustain dark respiration during nighttime, it is parameterized as a fraction of the CO_2 assimilation that would take place if radiation is not limited (Jacobs, 1994). The second respiration term represents all other respiration terms, including heterotrophic respiration from the soil and autotrophic respiration from the above- and below ground structural biomass (roots and stems). Since there is large uncertainty about the parameterization of the other respiration terms, we chose for a practical approach in C-TESSEL. The second term is referred to as the residual respiration R_{res} . Note that the magnitude of R_{res} is not smaller than the the magnitude of the dark respiration term, although its name might suggest otherwise. A temperature dependence function is used for

its parameterization:

$$R_{res} = R_{eco} - R_d = R_0 Q_{10}^{((T_{soil}-25)/10)} \quad (2)$$

where R_0 is the reference residual respiration at 25°C, T_{soil} is the temperature of the 2nd soil layer (°C) and Q_{10} is fixed at 2.0. R_0 is calibrated per vegetation type in each grid box assuming equilibrium between long term (multi-year) net CO₂ assimilation (A_n , equal to $A_g - R_d$), multi-year residual respiration and a prescribed annual amount of harvested biomass:

$$A_{n,acc} - harvest_{acc} = R_{res,acc} = R_0 (Q_{10}^{((T_{soil}-25)/10)})_{acc} \quad (3)$$

where subscript *acc* represents an accumulated value over a multi-year period. Table 1 gives the globally averaged yearly harvest estimates per vegetation class. For the calibration we ran the model offline using the 1 degree resolution global forcing for the 10-year period 1986-1995 from the second Global Soil Wetness Project (GSWP2, 2002). The estimates are based on a 40% carbon content of dry biomass (pers. comm. Calvet, 2005). In order to take harvest

Vegetation type	Harvest estimates
Deciduous	3.2
Coniferous	2.3
Evergreen	3.2
C ₃ grass	2.3
C ₄ grass	3.2
C ₃ crops	2.3
C ₄ crops	3.2

Table 1 : Globally averaged yearly harvest estimates ($t CO_2 ha^{-1} yr^{-1}$)

differences between climate zones into account, vegetation type specific harvest was distributed over the globe proportional to the 10-year locally averaged values of A_n . This procedure results in a climatological spatial distribution of R_0 . Also, the local NEE simulation for the Loobos site, discussed in Section 4, uses an R_0 value derived from the global equilibrium simulations.

Regarding soil moisture stress strategy, it is assumed that coniferous forests behave defensive, while the other vegetation classes use an offensive strategy (Calvet et al., 2004).

A major difference with TESSEL is the dynamic evolution of LAI. This affects the amount of evapotranspiration and interception. Also, in C-TESSEL, vegetation type specific monthly values of the roughness length are derived from ECOCLIMAP, whereas in TESSEL the roughness length is a grid-averaged constant value. As a consequence, the aerodynamic conductance in C-TESSEL is increased for high vegetation and reduced for low vegetation (Van den Hurk et al., 2000).

2.4 Stress regulation

As mentioned in Section 2.2, two types of soil moisture stress strategies are applied in the model. Coniferous forest is assumed to adopt the defensive strategy, in which the transpiration is reduced by stomatal regulation in case of drought. The offensive strategy is assigned to all other vegetation types.

The soil moisture effect on stomatal conductance is implemented via f_0 and D_{max} , parameters describing the effect of atmospheric humidity deficit on stomatal conductance. The air in the intercellular spaces of the plant is assumed to be saturated with water vapour, so the internal specific humidity (q_i) is equal to the saturation specific humidity at the leaf temperature (T_s). The difference between the humidity inside the plant and the humidity of

the ambient air at the leaf surface (q_s) is then given by the specific humidity deficit:

$$q_i - q_s = q_{sat}(T_s) - q_s = D_s \quad (4)$$

In the model, the effect of the humidity deficit on the stomatal conductance is applied via the ratio between the leaf internal concentration of CO_2 (C_i) and the concentration in the ambient air at the leaf surface ($C_s=353$ ppm), which is written as:

$$\frac{C_i}{C_s} = f + (1 - f) \frac{\Gamma}{C_s} \quad (5)$$

with

$$f = f_0 \left(1 - \frac{D_s}{D_{max}}\right) + f_{min} \left(\frac{D_s}{D_{max}}\right) \quad (6)$$

where Γ is the CO_2 compensation concentration and D_{max} is the maximum specific humidity deficit tolerated by the vegetation. When D_{max} is exceeded, the plant closes its stomata. f_0 is the value of f if $D_s = 0$, whereas f_{min} is the value of f when $D_s = D_{max}$. It is parameterized by:

$$f_{min} = \frac{g_c}{g_c + g_m} \quad (7)$$

Here, g_m is the mesophyll conductance used to describe the transport of CO_2 between the sub-stomatal cavity and the chloroplasts where the initial carbon fixation by the enzyme Rubisco takes place. g_c is the cuticular conductance allowing some diffusion of water vapour and CO_2 through the leaf cuticle, different from the main stomatal mechanism. The effects of f_0 and D_{max} on the stomatal conductance (g_s) are deduced from the following definition:

$$g_s = \frac{1.6 A_n}{C_s - C_i} \quad (8)$$

where the factor 1.6 represents the ratio between the diffusivities of water vapour and CO_2 . A_n is enhanced by high values of C_i (for the complete set of A-gs equations, we refer to Jacobs (1994) or Calvet et al. (1998)), which is positively correlated with f_0 (see Eqs. 5 and 6). From Eq. 5 it follows that the $C_s - C_i$ gradient is reduced for high values of f_0 . Both effects result in an increase of the stomatal conductance and transpiration when f_0 increases. The transpiration is also enhanced by high values of D_{max} , since the plant keeps its stomata open under higher atmospheric stress conditions. In the model, the influence of D_{max} is described by Eq. 6.

The transpiration is further enhanced by high values of g_m , allowing more CO_2 to diffuse to the chloroplasts. For high vegetation types, f_0 and D_{max} depend directly on g_m under conditions of soil moisture stress (referred to with an asterix). Calvet et al. (2004) present these relationships, based on a meta-analysis. For coniferous forest they are:

$$f_0^* = \frac{a - \ln(g_m^*)}{b} \quad (9)$$

$$D_{max}^* = -c \ln(g_m^*) + d \quad (10)$$

where $a = 4.7$, $b = 7$, $c = 37.97$, $d = 150.4$ and g_m^* is in mm s^{-1} .

For high vegetation types, values of g_m and f_0 are affected under conditions of soil moisture stress. For low vegetation types, the effect of soil moisture stress is applied to D_{max} instead of f_0 . Two regimes are distinguished: moderate stress and severe stress, separated by the critical soil moisture index value f_{2c} . In the model, f_{2c} is a vegetation type specific parameter

and its value does not depend on the applied stress strategy. Similar to TESSEL, the soil moisture index is given by the f_2 function:

$$f_2 = \frac{\bar{\theta} - \theta_{pwp}}{\theta_{cap} - \theta_{pwp}} \quad (11)$$

where the soil moisture at permanent wilting point θ_{pwp} and at field capacity θ_{cap} , are $0.171 \text{ m}^3\text{m}^{-3}$ and $0.323 \text{ m}^3\text{m}^{-3}$ respectively. $\bar{\theta}$ is a weighted average of the unfrozen soil water in the soil column (Van den Hurk et al., 2000). If $\bar{\theta}$ decreases to values below field capacity, the value of f_2 becomes smaller than 1 and stress occurs. For $f_2 > f_{2c}$, moderate soil moisture stress occurs. If $f_2 < f_{2c}$, the vegetation suffers from severe stress. The effect of the value of f_{2c} on the transpiration is presented schematically in Fig. 1. As can be seen in Fig. 1, the

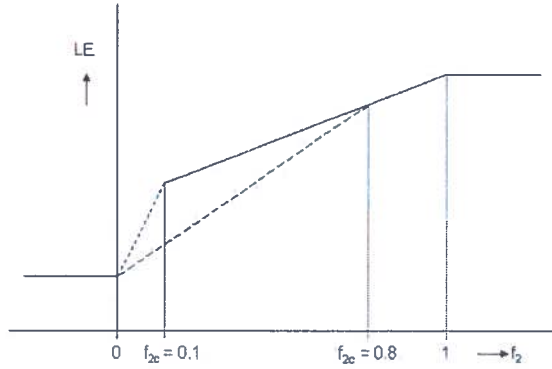


Figure 1 : Effect of f_{2c} on transpiration (here represented by LE). Two scenarios are assumed, one with $f_{2c} = 0.1$ and the other with $f_{2c} = 0.8$. The solid line represents the moderate stress regime. The severe stress regime is given by the dashed line.

reduction of the transpiration with decreasing f_2 is less for the moderate stress regime than for the severe stress regime. Furthermore, lower values of f_{2c} imply higher transpiration rates at low soil moisture content. In the model, this effect is obtained by the regulation of g_m and f_0 or D_{max} (Calvet, 2000; Calvet et al., 2004).

Coniferous forests (for which the model is validated in this paper) has a defensive stress strategy. It is modelled by an f_0 regulation in the moderate stress regime and a g_m regulation in the severe stress regime. Under moderate stress conditions, the transpiration is reduced by a decrease in the value of f_0 . Under severe stress conditions, a decrease in g_m overcompensates an increase in f_0 , thereby further reducing the transpiration.

3 Data sets and methods

In this study data from micrometeorological measurements at the coniferous forest site Loobos in the Netherlands (52 10'04" N; 5 44'38" E) are used. The site is part of the FLUXNET program network (Baldocchi, 2000) as well as the CarboEurope Integrated Project (Hofmann, 2006). The dominant tree species is Scots pine (*Pinus Sylvestris*). The grassy understory is ignored in the model. The site has a sandy soil. NEE and latent and sensible heat fluxes are measured by eddy correlation on a flux tower at a height of 26 m, with a 30 minute averaging interval following Aubinet et al. (2000). The displacement height is 8.1 m.

The model is driven by observed incoming shortwave and longwave radiation, wind speed, temperature, relative humidity and precipitation. A 95% fraction of coniferous forest is prescribed, adopted from ISBA-A-gs. The remaining 5% is bare soil. Other surface parameters like roughness length and background albedo come from the ECOCLIMAP database (Masson et al., 2003) at the Loobos location.

3.1 Validation strategy

The validation of C-TESSEL is performed for the years 1997-1999. During this period no significant soil moisture stress occurred. The forcing dataset is gap-filled in the framework of the FLUXNET program (Baldocchi, 2000). However, flux observations do have some gaps, especially in 1998 and 1999.

A spin-up experiment is performed, by iteration over the year 1996. After 3 iterations, values of the prognostic soil variables reached equilibrium. For the model output, we used time resolutions of both 30 minutes and 3 hours, depending on the output data analysis.

The validation considers CO_2 and daytime latent heat fluxes. The timing and amplitude of the diurnal and seasonal variation of the fluxes is investigated qualitatively. Regarding CO_2 fluxes, the NEE simulation is compared to observations. The simulated latent heat flux is compared to observations and to simulations by TESSEL.

In order to quantify the NEE performance of the model, we calculate the root mean square error (RMSE) based on daily averaged values of the 30 minute output and normalize this quantity to the observed mean. We split the time series into total, daytime (06:00-18:00 hrs local time) and nighttime (18:00-06:00 hrs local time) values. Only days for which the number of missing half hourly time slots in the observations is equal to or less than 6 within the day or night are taken into account. Furthermore, the summer and winter season are analyzed separately. Based on the NEE simulations, that show maximum uptake in June, the growing season is represented by the months May, June and July (MJJ). For winter simulations the months November, December and January (NDJ) are chosen. The normalized RMSE's are compared with the assumed observation accuracy. No uncertainty analysis on Loobos CO_2 flux measurements was available. Therefore, the observation accuracy is estimated based on an uncertainty analysis for an Amazonian forest (Kruijt et al., 2004). Uncertainties are associated mainly with nighttime fluxes (when wind speed is low), gap filling within the 30 minute interval, eddy correlation data processing and averaging. The observational uncertainty in nighttime fluxes is very large and may reach values up to 100%, depending on the specific methodology used for the evaluation of accuracy. The daytime uncertainty goes up to 35% when there is no precipitation. For Loobos this might be smaller, but would still be around 25%, from which 20% is estimated as random error and 5% as systematic error (pers. comm. Kruijt, 2006). For nighttime and daytime means, the random error decreases by the root of the number of time steps taken into account.

For the quantitative analysis of the simulated daytime latent heat flux, we use a similar approach as for NEE. Only the summer season is evaluated, since the latent heat flux is close to zero in winter. To be consistent with the NEE analysis, we use the months May, June and July (MJJ). For this period, the latent heat flux observational record contained more gaps than the NEE record. As a measure of the quantitative model skill, the RMSE values are compared with the observed variability, since no reliable estimates of the accuracy of latent heat flux measurements are available. However, it is expected that the latent heat flux can be measured with more accuracy than the NEE, since fast measurements of air humidity are easier to carry out than fast CO_2 concentration measurements.

3.2 Structure of the general sensitivity analysis

A general sensitivity analysis is carried out, in order to investigate the sensitivity of the simulated daytime latent heat flux to a number of parameters in the photosynthesis and LAI module. These are selected from the set of vegetation type specific parameters used in ISBA-A-gs (Gibelin et al., 2006). From this set, the assumed three crucial vegetation parameters are mesophyll conductance (unstressed with respect to soil moisture) g_m^* , critical soil moisture index f_{2c} and leaf nitrogen content N_a . They are considered to represent different mechanisms involved in latent heat flux simulation. Photosynthesis is represented by g_m^* , soil moisture dependence by f_{2c} and vegetation (LAI) by N_a (see Section 2.2). In the model structure, g_m^* is the only external vegetation type specific parameter representing photosynthesis. As pointed out in Section 2.4, f_0^* and D_{max}^* depend directly on g_m^* .

For the analysis, Loobos data for the years 1997 and 2003 are used, representing different soil moisture conditions. Little soil moisture stress occurred in 1997. 2003 had an anomalously dry summer, causing substantial soil moisture stress according to the simulations. In the analysis, gap-filled data are not taken into account. Only time steps between 10:00 and 14:00 hrs local time are selected in order to eliminate the influence of diurnal variation on the sensitivity analysis as much as possible. Furthermore, time steps with precipitation and with friction velocity (u_*) values lower than 0.1 m s^{-1} are not included.

The analysis is carried out in a Monte Carlo framework. C-TESSSEL is run 10000 times, each run having a unique combination of the parameter values that are generated randomly from a uniform distribution, with specified upper and lower limits (Table 2). Limits for g_m^* are

Parameter	Lower limit	Upper limit	Standard
g_m^* (mm s^{-1})	0.5	5.0	2.0
f_{2c} ($\text{m}^3 \text{ m}^{-3}$)	0.1	0.8	0.3
N_a (%)	0.3	6.0	2.8

Table 2 : *Parameter limits and standard value in C-TESSSEL*

deduced from Gibelin et al. (2006). Limits for N_a are chosen to vary symmetrically around the standard value. The f_{2c} limits are specified in a broad range, in order to detect enough sensitivity.

A spin-up is performed by running the model for the previous year. The computer data storage availability forced us to perform the spin-up with the ISBA-A-gs standard parameter set instead of with the randomly chosen set. The time step of the model output is 30 minutes, in order to capture the 10:00-14:00 hrs local time interval with sufficient temporal resolution.

The parameter sensitivity is evaluated by analyzing the bias and unbiased RMSE of the latent heat flux. The analysis of the bias gives insight in the sensitivity of the magnitude of the simulated flux to the selected parameters and also indicates the range of parameter values that gives the smallest bias. The unbiased RMSE is informative about the sensitivity of day-to-day variation in the simulated flux. Per day, values averaged for the 10 to 14 hrs period are used rather than 30 minute time slots in order to reduce scatter. Days are not taken into account if less than 6 out of 8 time steps satisfy the criteria for the observational data described above. As a result, the analysis is based on 283 days.

We follow the principles of the General Sensitivity Analysis method by Spear and Hornberger (1980). The 10000 simulations are ranked according to the bias or unbiased RMSE. Ten classes from low to high values are then defined, each having 1000 members. For each parameter, the relative cumulative frequency distribution of the parameter value within each class is plotted in one figure. A collapse of the curves into one straight line represents a uniform distribution of the parameter in all classes, implying that the parameter is insensitive. A large divergence of the ten distributions indicates strong sensitivity to the parameter.

4 Validation results

4.1 NEE

Fig. 2 shows the modelled and measured NEE averaged over 10 days for the 3-year period 1997-1999. The sign convention for CO_2 fluxes is positive upward, thus net CO_2 uptake leads

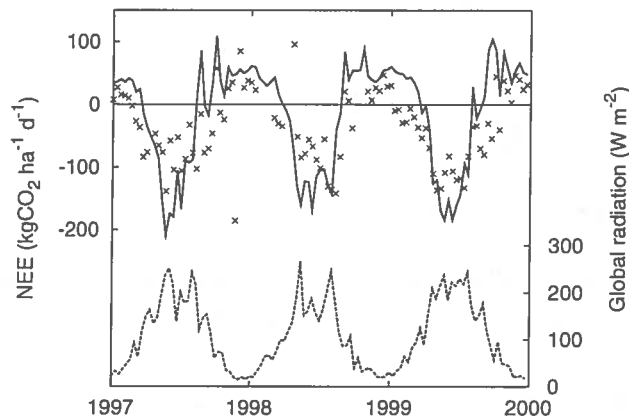


Figure 2 : 10-day averaged modelled NEE (solid line, positive upward), observed NEE (crosses) and global radiation (dashed line).

to negative NEE. In the lower part of Fig. 2, the global radiation is plotted. Outliers in NEE observations are the result of gaps in the data record, causing the 10-day averaged value to be based on a small number of data. In general, the model shows a similar seasonal variation pattern in NEE as the observations. However, C-TESSEL overestimates the downward NEE (CO_2 uptake) during summer and the upward NEE (CO_2 release) in late autumn and early spring. Also, the modelled onset of the growing season (when CO_2 assimilation starts to exceed respiration) is delayed as compared to the observations. After the winter radiation minimum, the NEE observations follow the radiation curve well, but the model NEE response to radiation is too slow. As will be described in Section 4.2, the simulated LAI is lower than is observed at the site at this moment in the year, causing an underestimation of CO_2 assimilation by the vegetation. At the same time, respiration starts to rise due to the temperature increase in spring (Eq.2). The increase in respiration partly compensates the too small increase in CO_2 assimilation. This can be seen in Fig. 3, showing the different components of NEE. In the growing season, the magnitude of the dark and residual respiration terms is comparable, whereas in winter only the residual respiration term contributes to the ecosystem respiration, due to the low CO_2 assimilation.

Fig. 4 provides more insight into the model response to global radiation and air temperature. NEE and its components are shown for 6 temperature classes as a function of global radiation. The gross CO_2 assimilation shows both a radiation and a temperature response whereas the respiration terms are only responsive to temperature. Since gross CO_2 assimilation values are much higher than respiration values, at least for the higher temperature classes, NEE is also seen to be responsive to both radiation and temperature.

The mean diurnal cycle of simulated NEE for the months June (growing season) and December (winter season) over the three years is compared to observations in Fig. 5. For the diurnal cycle, the amplitude of NEE is overestimated in June and underestimated in December. In June, carbon uptake during the day is overestimated by approximately a factor

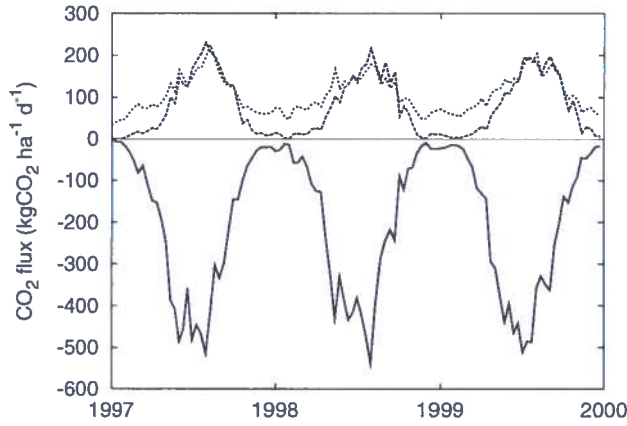


Figure 3 : 10-day averaged components of NEE (positive upward): gross CO_2 assimilation A_g (solid line), dark respiration R_d (dashed line) and residual respiration R_{res} (dotted line).

of 2. In winter both observations and simulations show ongoing photosynthetic activity around noon, owing to the fact that coniferous trees do not lose their needles. However, observations indicate a stronger CO_2 uptake. Note that the CO_2 flux is much smaller than in the growing season. In both months, nighttime respiration is overestimated. In June, the timing of the sign change of the net CO_2 flux in the morning and in the evening is simulated well by the model, whereas in December, the model simulates a shorter period around noon where net uptake of CO_2 occurs.

Table 3 presents the statistical information for the quantification of the model NEE performance (see Section 3.1). In general, the mean modelled and observed values have the

	MJJ night	MJJ day	MJJ total	NDJ night	NDJ day	NDJ total
number of days	255	268	264	202	213	203
model mean	210	-487	-142	79	21	50
observation mean	94	-272	-91	62	-7	28
bias	116	-215	-52	17	28	22
RMSE	135	256	80	27	39	29
RMSE/obs mean	1.43	-0.94	-0.88	0.44	-5.53	1.04

Table 3 : Statistics on daily averaged growing season (MJJ) and winter season (NDJ) NEE ($\text{kgCO}_2\text{ha}^{-1}\text{d}^{-1}$). The RMSE divided by the observation mean is referred to as normalized RMSE.

same sign except for the daytime NEE in the winter season. Table 3 confirms the model overestimation of CO_2 uptake during the day and the overestimation of CO_2 release during nighttime in the growing season. In general, the RMSE values are large. In NDJ the normalized RMSE during nighttime is 44% which is acceptable knowing that the uncertainty in 30 minute individual nighttime fluxes can be as high as 100% (Section 3.1). However, in MJJ, when values of respiration at night are higher than in winter, the normalized RMSE is 143%. During daytime in MJJ, the normalized RMSE is 94%, which is far more than the observational uncertainty of 25% argued in Section 3.1. The extremely high value of daytime normalized RMSE in NDJ (553%) is due to very low absolute values of NEE. Considering the 24 hours totals of NEE, we find values of the normalized RMSE close to 100% (88% for MJJ, 104% for NDJ). On the whole, NEE is not simulated within the observational uncertainty

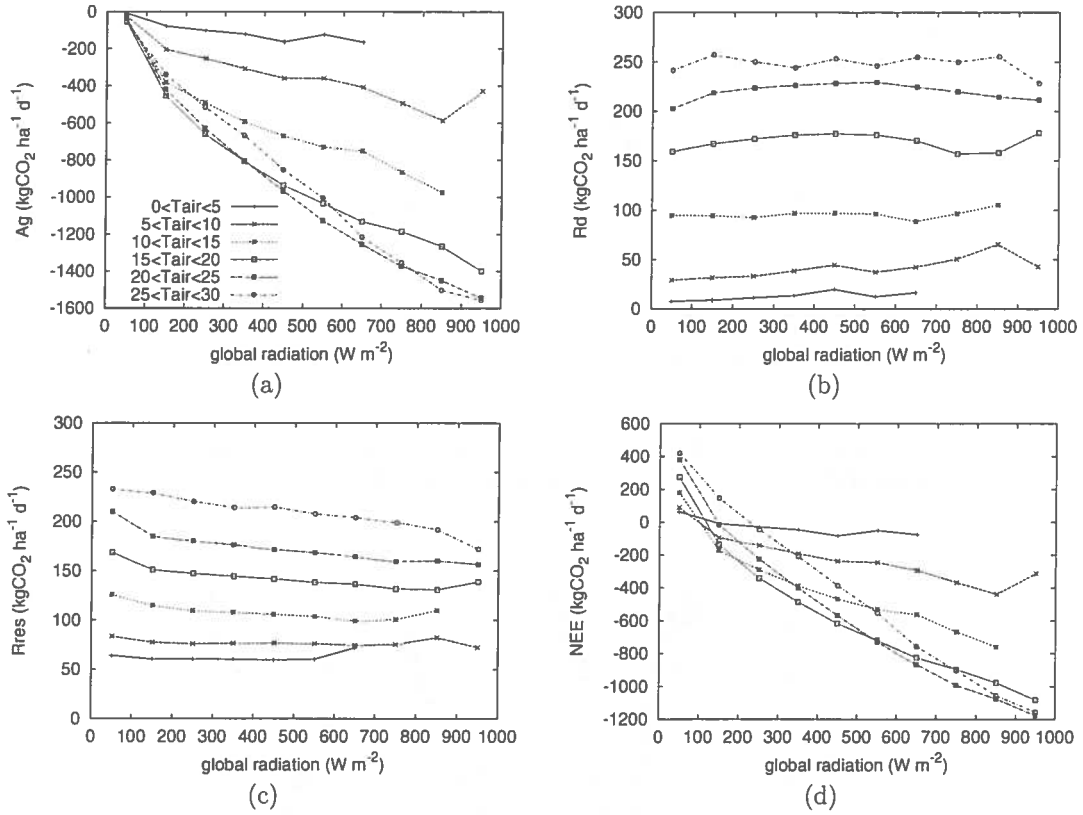


Figure 4 : CO_2 fluxes (positive upward) as a function of global radiation (in intervals of $100 W m^{-2}$) for 6 air temperature classes (listed in figure a). a: gross CO_2 assimilation A_g , b: dark respiration R_d , c: residual respiration R_{res} , d: NEE. Model output data with a 30 minute resolution are binned to global radiation classes and averaged per bin.

range for Loobos. The next section provides a link between the NEE and LAI simulations.

4.2 Latent heat flux and LAI

The latent heat flux for Loobos is simulated by both TESSEL and C-TESSEL. The sign convention for the latent heat flux is positive downward. Fig. 6 shows the 10-day averaged simulated daytime (06:00-18:00 hrs local time) latent heat fluxes. Note that quite a few gaps were present in the observations during the summer season, especially in 1998 and 1999. In spring, the C-TESSEL simulation lags the TESSEL simulation and the observations. In summer, C-TESSEL gives (slightly) higher latent heat flux values, closer to the observations.

A major difference between the models is the LAI. C-TESSEL calculates LAI interactively, whereas TESSEL does not show any seasonal variability (Fig. 7). Although C-TESSEL simulates a large seasonal LAI amplitude the latent heat flux simulated by TESSEL does not differ very much from the C-TESSEL simulation. In the winter period, when differences in LAI are highest, the latent heat flux is small. The latent heat flux is a combination of transpiration from vegetation and evaporation from the interception reservoir, bare soil and snow. Fig. 8 shows the separate contributions to the latent heat flux for both TESSEL and C-TESSEL. In winter, evaporation from the interception reservoir contributes most to the latent heat flux. In summer, the vegetation takes over. For both vegetation and interception,

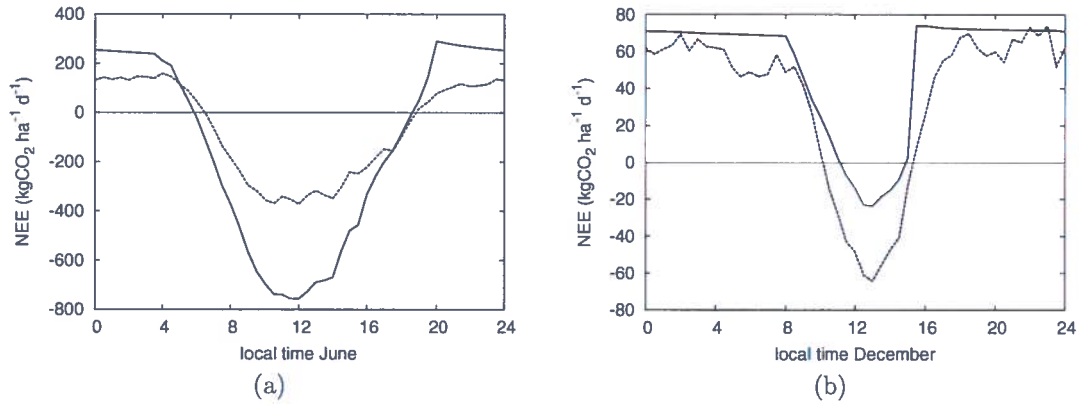


Figure 5 : Modelled (solid line) and observed (dashed line) NEE diurnal cycle (positive upward) averaged for the months June (a) and December (b).

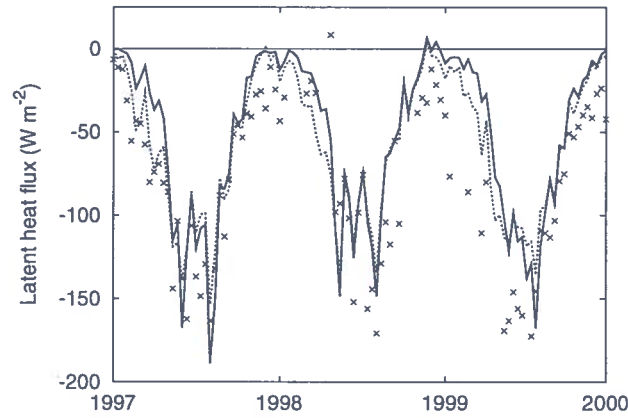


Figure 6 : 10-day averaged daytime latent heat flux (positive downward) simulated by TESSEL (dashed line) and C-TESSEL (solid line). The crosses represent the observations.

it is obvious that a higher LAI value is associated with more transpiration and evaporation. The lower C-TESSEL daytime latent heat flux in spring is caused by the lower LAI (Fig. 7), reducing both transpiration from the vegetation and evaporation from the interception reservoir. The higher C-TESSEL daytime latent heat flux in summer is due to the higher vegetation transpiration related to higher LAI (Fig. 7). However, compensation is provided by reduced bare soil evaporation due to reduced soil water content and reduced throughfall for higher LAI.

Table 4 presents the statistical information for the quantification of the model latent heat flux performance (see Section 3.1). Here, MJJ daily averaged daytime values are used. If we allow 6 missing time slots per day, only 54 days are taken into account in the analysis. If the number of allowed missing time slots is increased to 18, the number of days taken into account is 159. The normalized RMSE appeared insensitive to this choice, as did the ratio between the C-TESSEL and TESSEL bias (mean error). Therefore, we only present the statistics for the criterion of 6 missing time slots. Both models simulate a lower latent heat flux than observed. In comparison with observations, C-TESSEL has a smaller bias but higher RMSE for MJJ

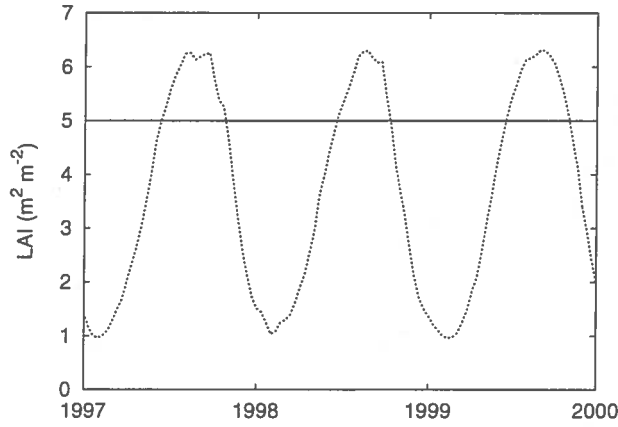


Figure 7 : Fixed LAI value of TESSEL (solid line) and the LAI simulated by C-TESSEL (dashed line).

C-TESSEL mean	-126
TESSEL mean	-116
observation mean	-151
C-TESSEL - observation bias	25
C-TESSEL - observation RMSE	56
C-TESSEL - observation normalized RMSE	-0.37
TESSEL - observation bias	36
TESSEL - observation RMSE	50
TESSEL - observation normalized RMSE	-0.33
C-TESSEL - TESSEL bias	-10
C-TESSEL - TESSEL RMSE	24
C-TESSEL - TESSEL normalized RMSE	-0.21

Table 4 : Statistics on MJJ daily averaged daytime latent heat flux (Wm^{-2}). Days are taken into account if the number of missing half hour time slots is 6 or less. The normalized RMSE is the RMSE divided by the reference mean.

than TESSEL. This means that on average, C-TESSEL simulates a higher flux in MJJ, but overestimates the day-to-day variation. Also, the normalized RMSE is larger for C-TESSEL than for TESSEL, although the differences are small.

For the evaluation of the RMSE, we need a measure of the variation within the observational dataset (Section 3.1). The day-to-day variation depends on meteorological variables such as global radiation, air temperature and humidity deficit. The standard deviation within the whole dataset of MJJ daily mean latent heat flux is to a large extent explained by global radiation. In order to eliminate this trend, the dataset is divided into two classes of global radiation that have equal numbers of observations. The standard deviations within both groups are averaged. For both radiation classes the standard deviation is normalized by the mean, as presented in Table 5. The standard deviation is larger for the low global radiation class. This indicates that for low radiation levels, other factors like temperature or humidity deficit have more influence on the latent heat flux than for high radiation levels. The average normalized standard deviation is -0.23. The normalized RMSE values of C-TESSEL and TESSEL (-0.37 and -0.33, respectively), exceed this accuracy estimate by 60% and 43%. Still,

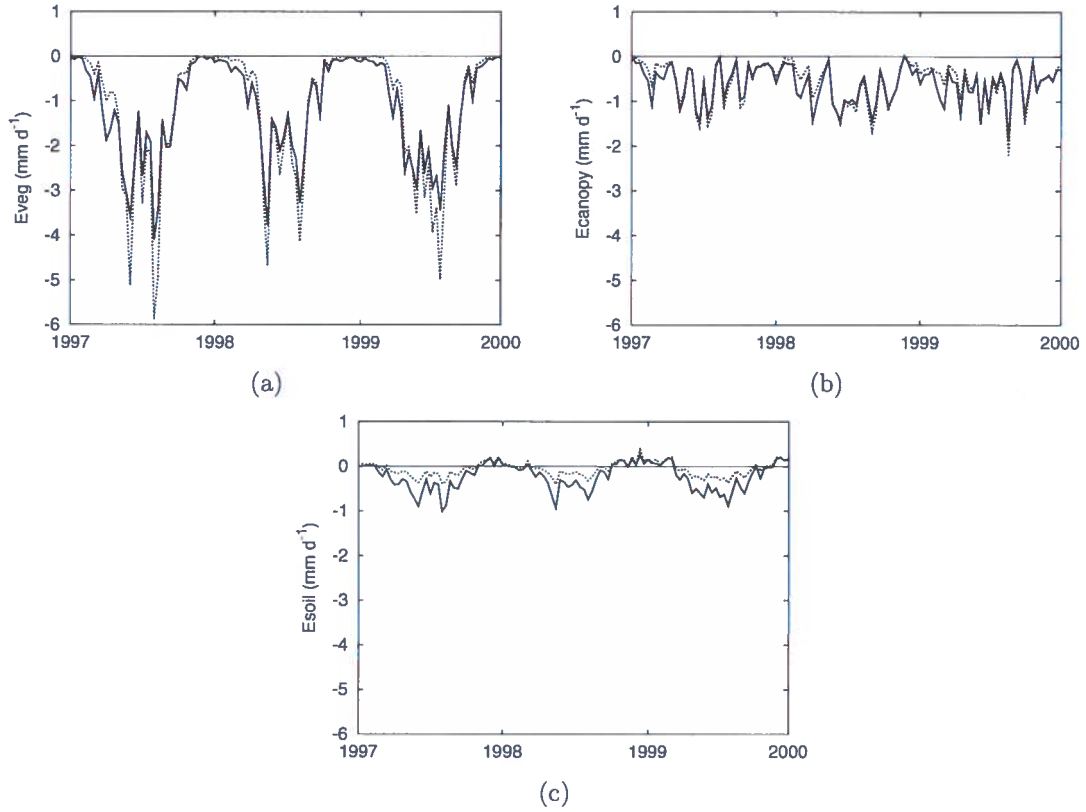


Figure 8 : 10-day averaged daytime evaporation (positive downward) simulated by TESSEL (solid line) and C-TESSEL (dashed line). a: vegetation, b: interception reservoir, c: bare soil.

the order of magnitude is comparable, indicating an acceptable model performance for the latent heat flux in summer.

The annual cycle of LAI simulated by C-TESSEL seems rather large for a coniferous forest that has needles all year round. Loobos site estimates indicate that the LAI of the coniferous trees ranges from 1.7 to 2.2 m^2m^{-2} , whereas the LAI of the understory varies from 0.0 to 1.1 m^2m^{-2} (Elbers, 2005). In the model, a 95% fraction of coniferous trees is assumed. This (probably) too high value influences the LAI value, but does not explain the large seasonal amplitude in the LAI simulation. Apparently, the modelled LAI response of coniferous forests to seasonal variation in meteorological conditions (like radiation and temperature) is too strong for the Loobos forest. In the NEE validation exercise, it became clear that the model overestimates the CO_2 uptake in the summer season. This may directly be linked to an overestimation of the LAI or vice versa.

5 General sensitivity analysis

The general sensitivity analysis is performed for two years. 1997 was a normal year, with little soil moisture stress. In 2003, Central and Western Europe experienced an anomalously warm and dry summer. In the model, soil moisture values for 2003 are indeed lower than for 1997. With the standard parameter values, the modelled 10-day averaged normalized soil

Global radiation classes	< median	> median
mean	-128	-175
standard deviation	40	26
normalized standard deviation	-0.31	-0.15

Table 5 : Statistics on MJJ daily averaged daytime latent heat flux observations (Wm^{-2}), divided into two global radiation classes. The normalized standard deviation is the standard deviation divided by the mean.

moisture index f_2 decreases to 0.65 in 1997 and to 0.35 in 2003. Soil moisture observations are not available for 1997 and 2003. However, latent heat flux observations from the Loobos site do not indicate that in 2003 severe soil moisture stress occurred, since the measured daytime latent heat flux values in the 1997 and 2003 summer are comparable. Beersma et al. (2004) conclude that in the Netherlands the summer of 2003 was relatively dry without being extremely dry. Also, NEE at Loobos was not reduced much in 2003 in contrast to many other forests in Europe (Ciais et al., 2005). However, since the soil moisture simulations for 1997 and 2003 differ significantly, the model sensitivity can still be evaluated for different soil moisture conditions.

The sign convention for the latent heat flux in the sensitivity study is positive upward, in contrast with the validation study. So, a negative bias implies that the model underestimates the flux. For the bias of the simulated latent heat flux, the relative cumulative frequency distributions of the three investigated parameters for 1997 and 2003 are presented in Fig. 9. The distributions for the unbiased RMSE are shown in Fig. 10. From both Figures it is clear that in 1997 and 2003 very similar distributions occur. So, apparently the different climatological conditions in 1997 and 2003 do not influence the sensitivity of the model parameters.

Figs. 9 and 10 show that the g_m^* value is uniformly distributed over the latent heat flux classes, indicating that the latent heat flux is insensitive to g_m^* . In Section 2.4, the functional relationships between f_0^* and D_{max}^* on the one hand and g_m^* on the other were described (Eqs. 9 and 10). The latent heat flux correlates positively with these three parameters. According to the negative log-relationships, lower values of g_m^* are compensated by higher values of f_0^* and D_{max}^* . These compensating effects limit the sensitivity of the latent heat flux to g_m^* .

Since the observational record is the same for each of the 10000 experiments, the distributions for the bias in Fig. 9 are equal to the distributions of the simulated magnitude of the latent heat flux. The latent heat flux is enhanced by high values of N_a , via the stimulating influence on LAI (see Section 2.2). As was explained in Section 2.4, the latent heat flux is also enhanced by low values of f_{2c} . Fig. 9 confirms these enhancements. In the highest bias classes, values of N_a and f_{2c} are on the high and low side respectively. In the lower classes, values of f_{2c} are more evenly distributed. Apparently, vegetation (N_a) is the main limiting factor for the lower magnitudes. In these lower classes, the sensitivity to the soil moisture conditions (f_{2c}) increases with increasing LAI. This can be seen from the uneven distribution of f_{2c} values in the higher classes. The sensitivity to N_a is high over the whole range of simulations.

The bias values range from $-68 W m^{-2}$ (the lower limit of class 1) to $10 W m^{-2}$ (the upper limit of class 10)(values are not shown in Fig. 9). The zero bias is present in class 8. Apparently, most combinations of parameter values result in an underestimation of the latent heat flux in Loobos. The smallest bias is obtained by f_{2c} values from 0.1 to 0.6 where the steepest part of the curve occurs between 0.4 and 0.5 (class 8). The standard parameter value of 0.3 seems to be quite good for Loobos. For N_a , values in class 8 range from 3 to 6% in 1997 and 2 to 6% in 2003 with a quite linear distribution. The standard parameter value of 2.8% is on the low side of the optimal range.

Fig. 10 gives an indication of the ability of the parameters to describe the day-to-day variation in the latent heat flux. Here, the optimal fit is obviously represented by the lowest class, indicating the lowest RMSE values. It is obvious that the day-to-day variation is best modelled by low values of N_a and high values of f_{2c} , although in 1997 the f_{2c} distribution of the lowest class is quite linear. This is in contrast with the parameter values that yield the lowest biases. Apparently, the model is not able to simulate the Loobos observed latent heat flux magnitude and day-to-day variation well at the same time. A small bias is accompanied by an overestimation of the day-to-day variation, whereas the latent heat flux is underestimated by parameter values that better describe the day-to-day variation.

6 Discussion and conclusions

With the newly developed C-TESSEL, simulations of net carbon and latent heat fluxes were performed for the Loobos coniferous forest site, located in the Netherlands. Generally, NEE is not simulated within the observational uncertainty range. The model overestimates both the CO_2 uptake during the growing season and the CO_2 release in winter. Linking the diurnal cycle simulations of NEE to the seasonal cycle, we find that the model overestimation of CO_2 uptake during the growing season is due to the overestimation of daytime CO_2 uptake. The model overestimation of CO_2 release in winter is due to the underestimation of photosynthetic activity during daytime and to a smaller extent to the overestimation of CO_2 release during nighttime. This may be caused by the overestimation of LAI in summer and underestimation in winter, respectively.

Besides the annual amplitude, also the timing of the diurnal and seasonal variation is evaluated. The simulated timing of the NEE sign change in the diurnal cycle during the growing season matches the observations very well. In winter however, observations indicate a longer period of net CO_2 uptake during daylight hours. Regarding the seasonal variation, the simulated sign change from net CO_2 release to net uptake in spring is delayed as compared to the observations, due to underestimation of LAI and thus CO_2 assimilation. This may also affect the soil temperature and therefore the residual respiration. If too much radiation reaches the surface, the temperature of the upper soil will be overestimated as well as the respiration. An analysis of chamber measurements of soil respiration from the Loobos site over the 2000-2006 period was carried out, in which R_0 and Q_{10} were optimized. Although the residual respiration in C-TESSEL also includes the respiration from the structural biomass, the analysis gives an indication of the temperature response of the respiration. The optimization yielded a higher Q_{10} value (3) and a lower R_0 value than applied in the model. This indicates that the model's temperature response is underestimated for Loobos, confirming the conclusion that the late onset of the growing season is due to an underestimation of CO_2 assimilation rather than an overestimation of CO_2 respiration.

Like the gross CO_2 assimilation, the simulated NEE responds to both radiation and temperature. Respiration, however, is only responsive to temperature in the model. A dependence on radiation would not allow the model to sustain dark respiration during nighttime. The lack of sensitivity of the dark respiration to radiation is questionable. However, one would expect a much closer relation with the actual gross CO_2 assimilation, since plants can only respire CO_2 after assimilating it. For example, in the terrestrial biosphere model ORCHIDEE (ORganizing Carbon and Hydrology in Dynamic EcosystEms), the autotrophic respiration is a function of temperature, CO_2 assimilation and biomass (Krinner et al., 2005).

The latent heat flux simulated by C-TESSEL does not differ much from the TESSEL simulation. Apparently, the interactive calculation of LAI and the photosynthesis based canopy conductance parameterization do not result in large latent heat flux changes compared to TESSEL. The RMSE of both the TESSEL and C-TESSEL simulated latent heat flux is in

the same order of magnitude as the observational variation.

The amplitude of the simulated LAI is too large for a coniferous forest that has needles all year round. This is confirmed by Loobos site estimates. Here, the model may be too responsive to the seasonal variation in meteorological conditions. The overestimation of the modelled CO₂ uptake during the growing season may directly be linked to the high LAI or vice versa. In practice, data assimilation of vegetation may reduce errors in NEE. However, lower LAI values result in slightly lower latent heat fluxes. Results from the validation exercise and general sensitivity study do not indicate that there is a need for reducing the simulated latent heat fluxes during the growing season.

The general sensitivity analysis showed that different soil moisture conditions do not seem to influence the sensitivity of the latent heat flux to the model parameters. The latent heat flux was insensitive to g_m^* . This is because of the compensating effects of f_0 and D_{max} (Eqs. 9 and 10). However, the latent heat flux may be sensitive to the parameters a , b , c and d in these equations.

The latent heat flux is sensitive to the leaf nitrogen content N_a , representing the vegetation influence. Only at high values of N_a , the latent heat flux is sensitive to the critical soil moisture index f_{2c} , representing the soil moisture influence. The smallest bias is obtained by N_a values larger than the standard value, whereas for f_{2c} , the standard value lies within the range of values that give a small bias. This indicates that the model with the standard parameter values underestimates the yearly averaged daytime latent heat flux in Loobos. Comparing the analysis of the bias and unbiased RMSE, it turned out that the model is not able to simulate the Loobos observed latent heat flux magnitude and day-to-day variation well at the same time. A small bias is accompanied by an overestimation of the day-to-day variation, whereas the average latent heat flux is underestimated by parameter values that better describe the day-to-day variation.

In this paper, C-TESSEL is only validated for a coniferous forest at one site. Future validation exercises should aim at all 7 vegetation types distinguished in the model and cover more micrometeorological sites per vegetation type. Nonetheless, this study presents a first indication of the skill of C-TESSEL. We conclude that the current model NEE performance for coniferous forests does not allow the current configuration of the model to be used in a data assimilation system. The deviation from the NEE observations indicate that too large systematic increments would be needed in the data assimilation system. Some improvement may be achieved by extending C-TESSEL with a soil carbon and wood (dead biomass) reservoir which allows respiration calculations for each of the carbon reservoirs. The current residual respiration calibration on the multi-annual net CO₂ assimilation will then not be required. There are, however, more concerns. The fact that the model is insensitive for the mesophyll conductance through dependencies of other photosynthesis parameters, makes it difficult to tune relevant parameters. In addition, the firm criterion to simulate both the right magnitude of the latent heat flux and the day-to-day variability to which the model was exposed in this study was not met. This indicates that for the present Loobos site another set of parameters or modelling concepts would be preferable. However, simultaneous tests at different locations may reveal other optimal parameter sets for similar canopy types. Systematic confrontation with spatially distributed data (which is enabled in the data assimilation system under design) may prove helpful in this optimization procedure.

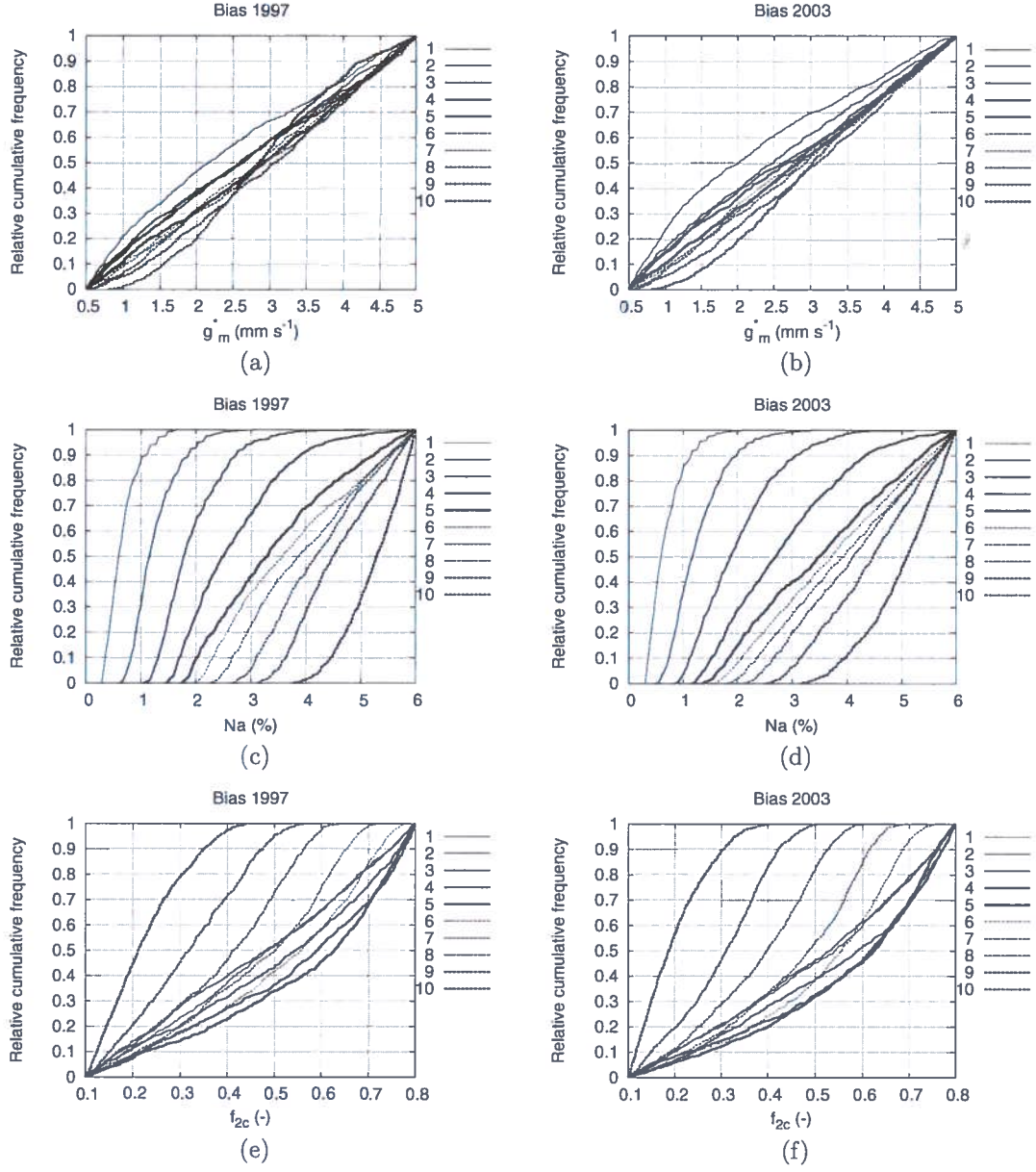


Figure 9 : Relative cumulative frequency distributions for the general sensitivity analysis on the latent heat flux bias. The 10 classes range from low (1) to high bias (10).

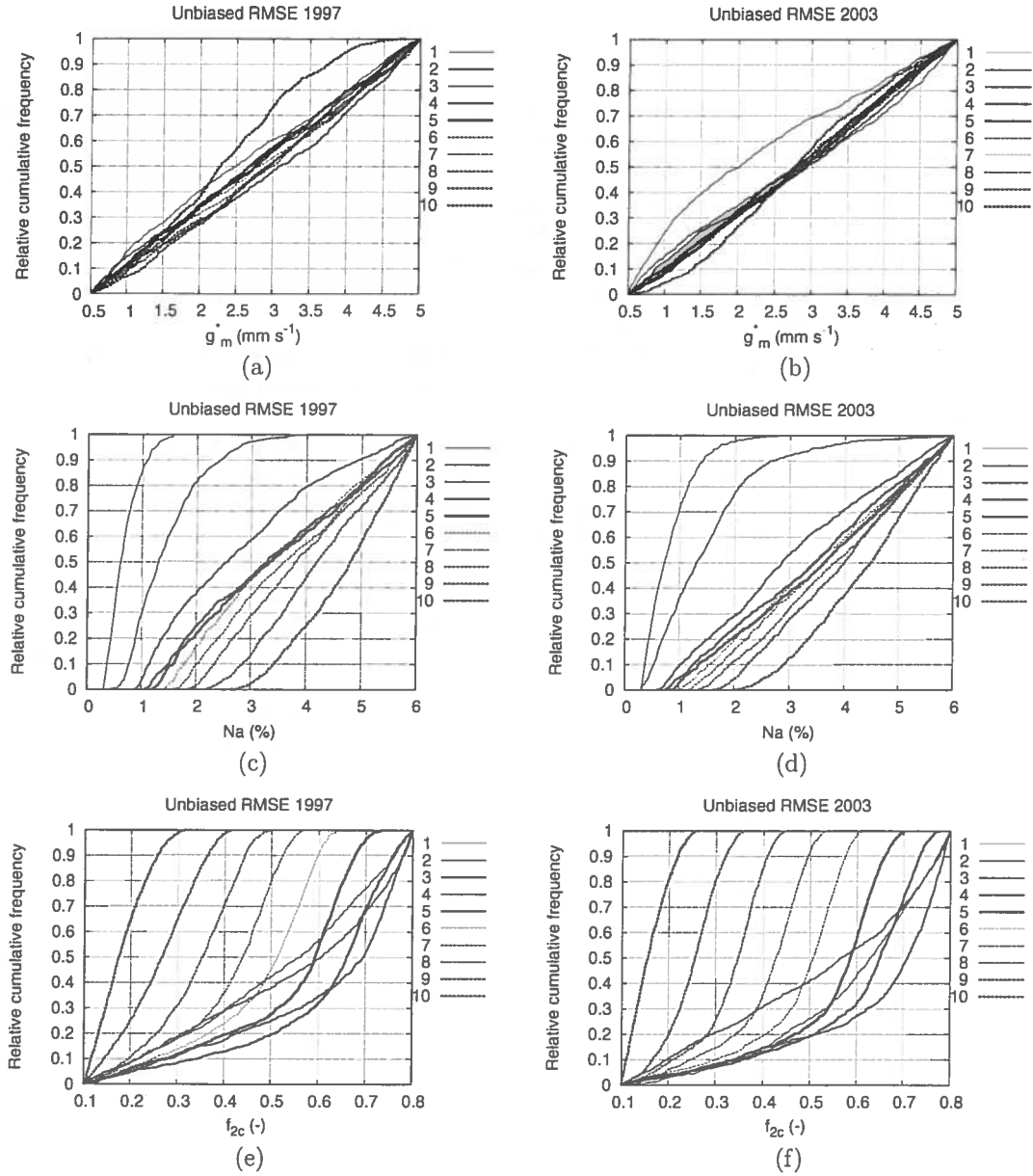


Figure 10 : Relative cumulative frequency distributions for the general sensitivity analysis on the latent heat flux unbiased RMSE. The 10 classes range from low (1) to high unbiased RMSE (10).

Acknowledgements

This study was cofunded by the European Commission within the GMES initiative in FP6, in the framework of the geoland integrated GMES project on land cover and vegetation.

References

- Aubinet, M., Grelle, A., Ibrom, A., Rannik, ., Moncrieff, J., Foken, T., Kowalski, A.S., Martin, P.H., Berbigier, P., Bernhofer, Ch., Clement, R., Elbers, J., Granier, A., Grnwald, T., Morgenstern, K., Pilegaard, K., Rebmann, C., Snijders, W., Valentini, R., Vesala, T., 2000. Estimates of the annual net carbon and water exchange of forests: the EUROFLUX methodology. *Adv. Ecol. Res.* 30, 113-175.
- Baldocchi, D., 2000. FLUXNET, A Global Network of Carbon, Water and Energy Flux Measurement Sites: A Continuation Proposal for the Project Science Office. NASA Research Announcement, NRA-00-OES-08.
- Beersma J.J., Buishand, T.A., Buiteveld, H., 2004. Droog, droger, droogst; KNMI/RIZA-bijdrage aan de tweede fase van de Droogtestudie Nederland. KNMI-publicatie 199-II, KNMI, De Bilt.
- Bonan, G.B., 1998. The land surface climatology of the NCAR land surface model coupled to the NCAR community climate model. *J. Climate* 11, 1307-1326.
- Calvet, J.-C., Noilhan, J., Roujean, J.-L., Bessemoulin, P., Cabelguenne, M., Olioso, A., Wigneron, J.-P., 1998. An interactive vegetation SVAT model tested against data from six contrasting sites. *Agric. For. Met.* 92, 73-95.
- Calvet, J.-C., 2000. Investigating soil and atmospheric plant water stress using physiological and micrometeorological data. *Agric. For. Met.* 103, 229-247.
- Calvet, J.-C., Soussana, J.-F., 2001. Modeling CO₂-enrichment effects using an interactive vegetation SVAT scheme. *Agric. For. Met.* 108, 129-152.
- Calvet, J.-C., Rivalland, V., Picon-Cochard, C., Guehl, J.-M., 2004. Modelling forest transpiration and CO₂ fluxes - response to soil moisture stress. *Agric. For. Met.* 124, 143-156.
- Ciais, Ph., Reichstein, M., Viovy, N., Granier, A., Oge, J., Allard, V., Aubinet, M., Buchmann, N., Bernhofer, Chr., Carrara, A., Chevallier, F., De Noblet, N., Friend, A.D., Friedlingstein, P., Grnwald, T., Heinesch, B., Keronen, P., Knohl, A., Krinner, G., Loustau, D., Manca, G., Matteucci, G., Miglietta, F., Ourcival, J.M., Papale, D., Pilegaard, K., Rambal, S., Seufert, G., Soussana, J.F., Sanz, M.J., Schulze, E.D., Vesala, T., Valentini, R., 2005. Europe-wide reduction in primary productivity caused by the heat and drought in 2003. *Nature* 437, 529-533.
- Cox, P.M., Betts, R.A., Jones, C.D., Spall, S.A., Totterdell, I.J., 2000. Acceleration of global warming due to carbon-cycle feedbacks in a coupled climate model. *Nature* 408, 184-187.
- Cramer, W., Bondeau, A., Woodard, F.I., Prentice, I.C., Betts, R.A., Brovkin, V., Cox, P.M., Fisher, V., Foley, J.A., Friend, A.D., Kucharik, C., Lomas, M.R., Ramankutty, N., Sitch, S., Smith, B., White, A., Young-Molling, C., 2001. Global response of terrestrial ecosystem structure and function to CO₂ and climate change: results from six dynamic global vegetation models. *Global Change Biology* 7, 357-373.
- Elbers, J., Loobos Site, Alterra, last page revision 26-05-2005, accessed 28-07-2006, <http://www.alterra-research.nl/pls/portal30/docs/folder/carboeurope.loobos/carboloo/loobos.htm>
- Friedlingstein, P., Dufresne, J.L., Cox, P.M., Rayner, P.M., 2003. How positive is the feedback between climate change and the carbon cycle? *Tellus* 55B, 692-700.

- Gibelin, A.-L., Calvet, J.-C., Roujean, J.-L., Jarlan, L., Los, S., 2006. Ability of the land surface model ISBA-A-gs to simulate leaf area index at the global scale: comparison with satellites products. *J. Geoph. Res.* 111, D18102, doi:10.1029/2005JD006691.
- GSWP2, 2002. Science and implementation plan gswp2. IGPO Publication Series 37.
- Hofmann, Y., CarboEurope IP website, last page revision 22-08-2006, accessed 20-09-2006, <http://www.carboeurope.org>
- Houghton, J., Ding, Y., Griggs, D., Noguer, M., Van der Linden, P., Dai, X., Maskell, K., Johnson, C. (Eds.), 2001. *Climate Change 2001: The Scientific Basis. Contribution of Working Group I to the Third Assessment Report of the Intergovernmental Panel on Climate Change*. Cambridge University Press, Cambridge, UK and New York, NY, USA.
- Jacobs, C.M.J., 1994. Direct impact of CO₂ enrichment on regional transpiration. Ph. D. Thesis, Agricultural University, Wageningen
- Jarvis, P.G., 1976. The interpretation of the variations in leaf water potential and stomatal conductance found in canopies in the field. *Phil. Trans. R. Soc. London B.* 273, 593-610.
- Knorr, W., Cox, P., 2004. CAMELS-Carbon Assimilation and Modelling of the European Land Surface. In: Bergamaschi, P., Behrend, H., Jol, A. (Eds.) *Inverse modelling of national and EU greenhouse gas emission inventories*. European Commission Joint Research Centre, Ispra, pp 66-69.
- Krinner, G., Viovy, N., De Noblet, N., Oge, J., Polcher, J., Friedlingstein, P., Ciais, P., Sitch, S., Prentice, I.C., 2005. A dynamic global vegetation model for studies of the coupled atmosphere-biosphere system, *Global Biogeochemical Cycles* 19, GB1015, doi:10.1029/2003GB002199.
- Kruijt, B., Elbers, J., von Randow, C., Araujo, A.C., Culf, A., Bink, N.J., Oliveira, P.J., Manzi, A.O., Nobre, A.D., Kabat, P., 2004. Aspects of the robustness in eddy correlation fluxes for Amazon rainforest conditions. *Ecological Applications* 14, S101-S113.
- Masson, V., Champeaux, J.-L., Chauvin, F., Meriguet, C., Lacaze, R., 2003. A global database of land surface parameters at 1-km resolution in meteorological and climate models. *J. Climate* 16, 1261-1282.
- Rayner, P. J., Scholze, M., Knorr, W., Kaminski, T., Giering, R., Widmann, H., 2005. Two decades of terrestrial carbon fluxes from a carbon cycle data assimilation system (CCDAS). *Global Biogeochemical Cycles*, 19 (2): GB2026, doi:10.1029/2004GB002254.
- Spear, R.C., Hornberger, G.M., 1980. Eutrophication in Peel Inlet II. Identification of critical uncertainties via Generalised Sensitivity Analysis. *Water Res.* 14, 43-49.
- Van den Hurk, B.J.J.M., Viterbo, P., Beljaars, A.C.M., Betts, A.K., 2000. Offline validation of the ERA40 surface scheme. ECMWF TechMemo. 295, 42 pp., ECMWF, Reading.
- Viovy, N., 2002. Description of the PILPSC-1 experiment. <http://www.pilpsc1.cnrs-gif.fr>

